EES Solar

PAPER

View Article Online
View Journal



Cite this: DOI: 10.1039/d6el00022c

# Interface intercalation into perovskite layer improving performance of tin perovskite solar cells

Muhammad Okash Ur Rehman, †[a] Debendra Prasad Panda, †[a] Wolfram Hempel,[b] Rabeb Issaoui,[a] Madineh Rastgoo,[a] Alwani Imanah Rafieh,[c] Valerio Stacchini,[c] Lorenzo Miele,[a] Enrica Luzzi,[a] Luigi Sanguigno,[a] Paolo Aprea,[a] Meng Li,[d] Guixiang Li,[e] Zafar Iqbal *[c] and Antonio Abate *[ac]

Received 9th February 2026
Accepted 6th April 2026

DOI: 10.1039/d6el00022c

rsc.li/EESSolar

The interfaces play a critical role in determining the performance and stability of perovskite solar cells (PSCs). In this work, we introduce a buried interface engineering strategy using phenylethylammonium iodide (PEAI), which subsequently diffuses into the famadinium tin iodide ($FASnI_3$) perovskite layer. This improves the perovskite crystallisation process, resulting in reduced lattice microstrain and better film microstructure. Consequently, the nonradiative recombination is supressed, suggesting an improved charge carrier dynamics. This approach is particularly effective for tin perovskites processed without dimethyl sulfoxide (DMSO), where controlling crystallisation remains a major challenge. DMSO-free tin-PSC devices fabricated using this strategy deliver a power conversion efficiency exceeding 11%, retaining 90% of their initial efficiency after 3500 hours of storage. These findings underscore the critical role of buried interface engineering in regulating bulk properties, marking a significant advancement in the development of efficient and stable tin-PSCs.

**Broader context**

Solar energy is considered clean energy and is expected to augment the world's energy supply in the future. In this context, perovskite solar cells (PSCs) are considered the most promising candidates for their ease of fabrication. However, there is a need to design the interfaces to approach the theoretical limit for these types of materials, as the main energy losses come from the interfaces. The most commonly used technique is the passivating strategy towards stability and high-efficiency devices. Here, we report an interface design by a 2D passivation layer that intercalates in the perovskite layer that offers better crystallization dynamics and trap free interface. This strategy will be helpful for interface design for tin perovskite solar cell, where crytalliazion is one of the challenges.

## Introduction

The global need for sustainable energy solutions has increased the demand for renewable energy sources worldwide. Among emerging technologies, perovskite solar cells (PSCs) have garnered considerable attention as a promising next-generation photovoltaic technology due to their high efficiency and cost-effectiveness.[1–3] The power conversion efficiency (PCE) of PSCs has shown a substantial improvement from 3.8% to over 27% due to the exceptional properties of perovskite materials, such as tunable band gaps, high absorption coefficient, and long charge carrier diffusion lengths and lifetime.[4–9] However, the constituent metal lead (Pb) is recognised as one of the most toxic elements to both the environment and human health, due to its ability to mimic calcium in biological systems and its severe impact on neurological development.[10,11] Furthermore, the high costs associated with the recycling of lead-PSCs compromise their viability for real-world applications, thus highlighting the need to explore lead-free alternatives to improve sustainability and minimise environmental impact.[12–14] Tin shares similar physicochemical properties with lead, as both belong to the same group in the periodic table, making it a viable substitute. With the advantage of a narrower bandgap, Eg, high carrier mobility, low exciton binding energy, and reduced toxicity, tin-PSCs have emerged as the most promising substitute.[15–17]

Tin-PSCs have recently achieved a certified PCE of over 17.71%, indicating a significant advancement in the field; however, they still lag behind their lead-based counterparts.[18–20]

[a]Department of Chemical, Materials and Industrial Production Engineering, University of Naples Federico II, 80125 Naples, Italy. E-mail: antonio.abate@unina.it; antonioabate83@gmail.com

[b]Zentrum für Sonnenenergie und Wasserstoff-Forschung Baden-Württemberg (ZSW), Meitnerstraße 1, 70563 Stuttgart, Germany

[c]Solar Energy Divison, Helmholtz-Zentrum Berlin für Materialien und Energie (HZB), Hahn-Meitner-Platz 1, 14109 Berlin, Germany. E-mail: zafar.iqbal@helmholtz-berlin.de

[d]Key Lab for Special Functional Materials of Ministry of Education, School of Nanoscience and Materials Engineering, Henan University, Kaifeng, 475004, China

[e]School of Materials Science and Engineering, Southeast University, Nanjing, 211189, Jiangsu, China

† Authors contributed equally.

Their performance is significantly hindered by self p-doping, which is caused by the oxidation of $Sn^{2+}$ to the unwanted $Sn^{4+}$.[21,22] Previously, it has been demonstrated by both our research group and Saidaminov *et al.* that dimethyl sulfoxide (DMSO), a commonly used solvent in the perovskite solar cells, is contributing to tin oxidation.[23,24] This uncontrolled oxidation has been a critical challenge in achieving lab-to-lab reproducibility.[25] In addition, DMSO causes microstructural voids, catalyses the deprotonation of A-site organic cation, and coordinates with iodide and extracts it from the perovskite lattice, altogether limiting the photovoltaic performance. To address such detrimental effects of DMSO, we demonstrated an alternative solvent system, a mixture of DEF (*N*,*N*-diethylformamide) and DMPU (*N*,*N*′-dimethylpropyleneurea) for tin-PSC fabrication, which outperformed the DMSO-based devices without any reducing agents or passivants.[26,27] Importantly, the usage of this solvent system prevents the $Sn^{2+}$ oxidation, resulting in no detectable $Sn^{4+}$.[28] Recently, we have achieved a PCE of 9.1% using perfluoroarene-based molecules to form a 2D/3D heterostructure at the top interface of the DEF : DMPU-based tin perovskite.[29] Hence, further research is needed to enhance the performance of non-oxidising solvent-based tin-PSCs, which hold the potential for efficient and stable tin-PSCs.

In addition to the low oxidation barrier, the rapid crystallisation of tin perovskites, a consequence of the high Lewis acidity of $Sn^{2+}$, results in a high defect density and random grain orientation.[30,31] Various strategies, such as additive engineering and top and bottom interface modifications, have been adopted to improve the crystallisation dynamics. Importantly, the perovskite/charge transport layer interface plays a critical role in the charge carriers extraction, thereby boosting photovoltaic performance.[32–34] In addition, it controls the crystallisation dynamics, resulting in suppression of defect density. The interface can be modified by forming a 2D/3D perovskite heterostructure through introduction of phenylethylammonium ($PEA^+$) salts either as an interlayer or additive in precursor solution, which improves the photovoltaic performance.[35–39] To improve the morphology and crystallinity of the perovskite, $NH_3SO_3$ has been employed as an addition to enhance the device performance.[40–43] The devices without encapsulation exhibit excellent long-term stability, and the PCE has increased from 13.08% to 16.02% for the champion device.[44] Wang *et al.* used 4-bromo-2,6-diaminopyridine (4BrDP) as a multifunctional additive for Sn-based perovskite, which enables a champion power conversion efficiency (PCE) of 13.40% by improving the film quality.[45] Given that DMSO-free tin-PSC is still in its infancy, we applied this strategy to enhance its performance.

In this work, we have introduced a unique interface diffusion strategy, where bulky $PEA^+$ cations from the bottom interface of perovskite diffuse into the bulk during film formation. To ensure the diffusion process, PEAI was spin-coated using the same non-oxidising solvent system as the perovskite precursor solution, DEF : DMPU (6 : 1 v/v). This approach enhances the crystallisation dynamics, evidenced form improved microstructure and reduced lattice microstrain. In addition, it suppresses the defect density and slows down the charge carrier recombination. Using these approaches, we have achieved a state-of-the-art PCE of 11% for DEF : DMPU-based tin-PSCs. Furthermore, these devices demonstrated excellent long-term stability retaining 90% of their initial efficiency after 3500 hours of storage in $N_2$ atmosphere, indicating the critical role of eliminating DMSO and interface modifications.

## Results and discussion

The interface of perovskite often suffers from poor crystallisation, defect accumulation, and energy level mismatch, limiting the device performance.[46,47] We have introduced a bulky organic cation, phenylethylammonium ($PEA^+$) cation at the bottom of the perovskite layer (Scheme 1). First, time-of-flight measurements were applied to probe the introduction of PEAI layer. We have measured the control device stack with configuration (glass/ITO/PEDOT-complex/$Al_2O_3$/$FASnI_3$/$C_{60}$/BCP) and target configuration (glass/ITO/PEDOT-complex/$Al_2O_3$/PEAI/$FASnI_3$/$C_{60}$/BCP). We have used a Cs-cluster to detect both positive and negative ions in this measurement so that all layers could be addressed (see details in SI). The $C_{60}$ and BCP layer was described by the $Cs_3C_2^+$-cluster, $FASnI_3$ by $CH_5N_2^+$, $Sn^+$ and $CsI^+$, EDAI by $C_2H_9N_2^+$, $Al_2O_3$ by $Al^+$, PEDOT by $Cs_3C_2S^+$, ITO by $In^+$ and glass by $Si^+$. For a better understanding, sputter time was transformed to a normalized depth and the detected signals were normalized to the maximum value (Fig. 1). The depth 0–1 covered the C60 and BCP layer, 1–2 the $FASnI_3$ absorber, 2–3 the $Al_2O_3$ layer, 3–4 the PEDOT and 4–5 finally the ITO. PEAI was identified by the fragment $C_8H_9^+$, which lost the ammonium group. There is no signature of PEAI in the control devices as shown in Fig. 1b. In contrast, in the target devices, PEAI is located at both the bottom and bulk region of $FASnI_3$, indicating its incorporation into the perovskite. We infer that PEAI layer partially diffuses into the perovskite bulk during the spin-coating process due to solvent miscibility and distributes non-homogeneously. This incorporation of PEAI improves the crystallisation dynamics, followed by a decrease in grain boundary defect density, resulting in improved interfacial carrier dynamics without altering the energy level alignment at the interface, as discussed in the subsequent sections.

To elucidate the influence of PEAI diffusion on crystallisation behaviour, we performed X-ray diffraction (XRD) measurements, and the resulting diffraction patterns. $FASnI_3$ crystallises in a cubic structure with the $Pm\bar{3}m$ space group, which is preserved following the incorporation of PEAI at the buried interface. No additional diffraction peaks were observed after PEAI treatment, confirming the absence of secondary phases or impurity. PEAI is generally known to form a thin two-dimensional (2D) perovskite layer at the interface. However, in this case, no distinct reflection was detected at lower $2\theta$ values, suggesting that the 2D perovskite phase either did not form or remains below the detection limit of the instrument. For further understanding of the microstructural impact of PEAI incorporation, Le Bail fitting was carried out on the diffraction data (Fig. 2a) to extract the microstrain values of the films. Strain is defined as the relative change in the dimensions of a material in

 

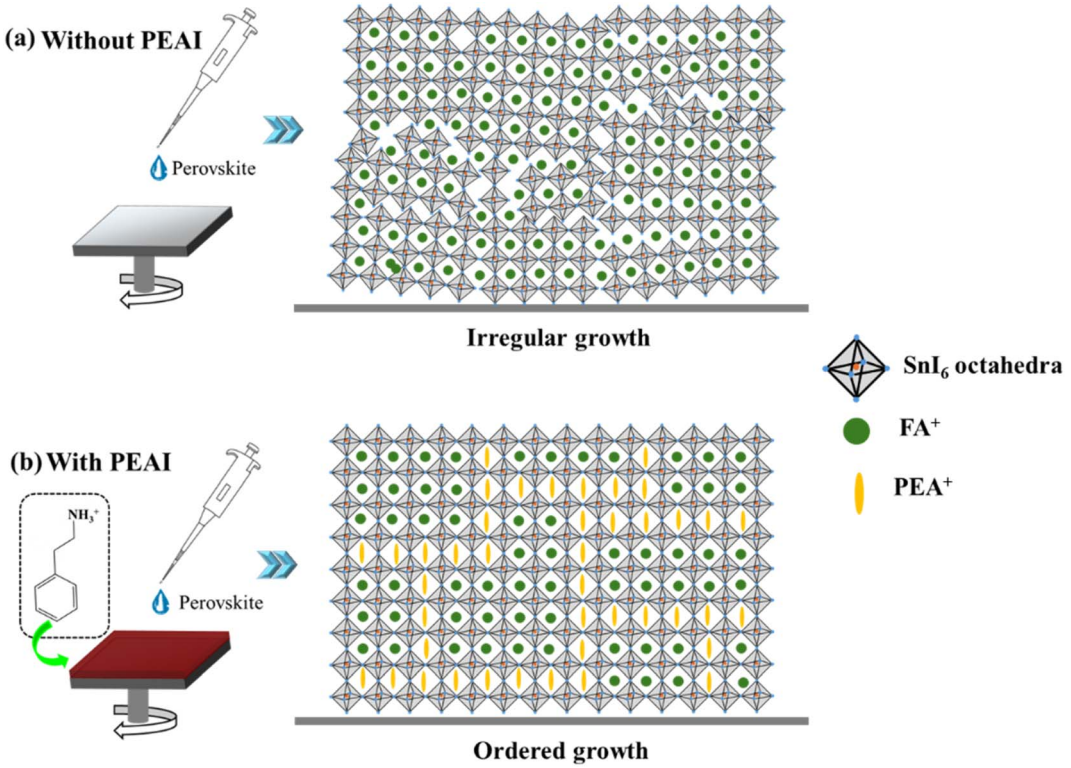


Scheme 1 A schematic representation of buried interface modifications of tin-PSCs by introducing PEAI at buried interface: (a) higher defect density at the bottom interface of perovskite without the PEAI interlayer. (b) Defect passivation by introducing PEAI at the bottom interface.

response to external forces. In crystalline solids, microstrain arises from local lattice distortions, typically induced by structural defects and crystallographic imperfections.[48] Following the introduction of the PEAI interlayer, the microstrain decreased from 11.5% to 7.7% (Fig. 2b), indicating a reduction in lattice disorder and an enhancement in crystal ordering. This improvement in structural quality is further supported by the narrowing of the full width at half maximum (FWHM) of the XRD peaks. Specifically, the FWHM of the first diffraction peak decreased from 0.123° in the control film to 0.115° in the PEAI incorporated film (Table S1), reflecting improved crystallinity.

The crystallisation dynamics are further supported by performing scanning electron microscopy (SEM) measurement and the top view images of control and target films are presented in (Fig. 2c). A significant increase in average grain size is observed, from 188 nm in the control film to 271 nm in the PEAI-diffused film. Statistical analysis confirms that the target films exhibit an improved microstructure with larger grain domains (Fig. S1). In addition, we conducted a cross-sectional SEM analysis to examine the variation in perovskite thickness. This resulted in a significant increase in the average film thickness from 234.1 nm in control to 310.9 nm in the target film (Fig. S2). This enlargement in grain size and film thickness can be attributed to a slower crystallisation rate induced by the PEAI interlayer, which facilitates more ordered crystal growth and contributes to improved photovoltaic performance. In general, surface roughness enhances the self-nucleation process due to a higher nuclei density in the vicinity of rough regions.[49] We believe that the introduction of PEAI salt as a bottom layer increases the surface roughness, acting as a site for nucleation. This lowers the energy barrier for crystallisation, thereby enhancing the crystallisation dynamics, which in turn leads to improved microstructure and photovoltaic performance. Collectively, the non-uniform distribution of PEAI in perovskite layer, intense diffraction peaks without shifting the peak position and enganced grain sizes suggest that PEAI is not affecting the perovskite crystal lattice. Rather it passivates vacancy and grain boundary defects.

We have employed steady-state photoluminescence spectroscopy (stPL) for control and target thin films, employing an excitation wavelength of 520 nm LEDs inside the $N_2$-filled glove box. These films were deposited on the glass substrates. Both control and target films exhibit a similar emission spectrum with a maximum of around 851 nm (Fig. 3a), which is in agreement with the previous report.[50] With PEAI diffusion, the target film shows higher photoluminescence intensity compared to the pristine $FASnI_3$ sample, suggestive of reduced defect density in the PEAI-modified films. This reduction in defects can be attributed to the improved crystallinity, as evidenced by the relaxed lattice microstrain and enlarged grain size. Further, the transient photoluminescence (trPL) measurements were conducted on the sample deposited on PEDOT/$Al_2O_3$ as a substrate (Fig. 3b and S3). The trPL spectra follows a decay that has been fitted with the bi-exponential equation (details in SI). The target film demonstrates a longer average PL lifetime (35.8 ns) than the control film (26.1 ns),

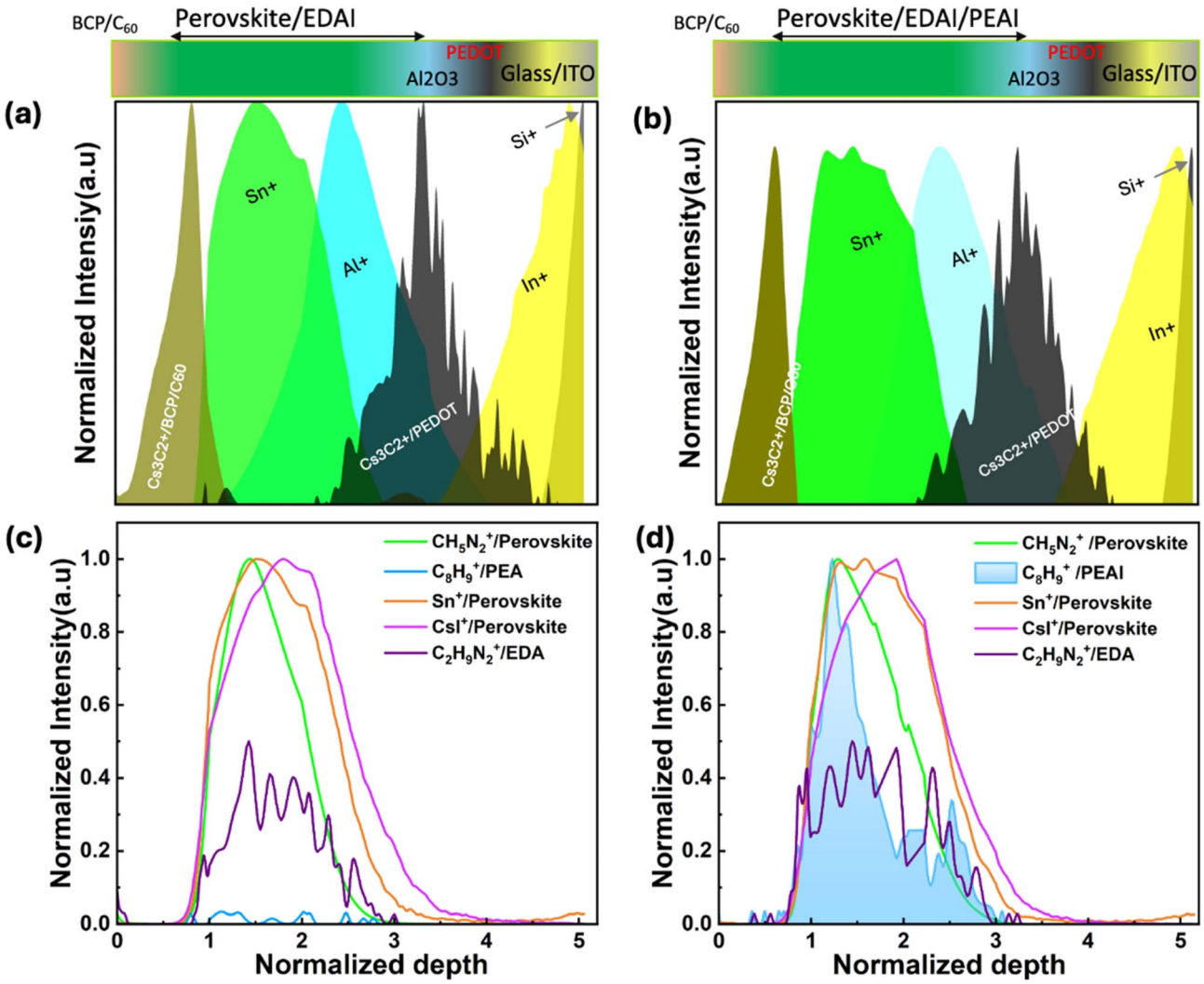


Fig. 1 Normalized ToF-SIMS depth profile measured with Cs-gun: (a) selected species for the control device stack (glass/ITO/PEDOT-complex/$Al_2O_3$/$FASnI_3$/$C_{60}$/BCP) with their respective fragments. (b) $FASnI_3$ perovskite region of the control device stack with $EDAI_2$ (ethylene diammonium diiodide) as an additive. (c) Selected species for the target device stack (glass/ITO/PEDOT-complex/$Al_2O_3$/PEAI/$FASnI_3$/$C_{60}$/BCP) with their respective fragments. (d) $FASnI_3$ perovskite region of the target device stack containing $EDAI_2$ as an additive with PEAI located in the perovskite region of the stack.

indicating less interfacial non-radiative recombination upon PEAI introduction. The suppression in non-radiative recombination originating from the decrease in defect densities, leading to enhancement of PL lifetime.

We further focused our investigations on the interface and its charge-selective properties. Charge extraction is a crucial parameter for an interface, which depends on its quality. To access this, we employed the transient surface photovoltage technique (trSPV) that was introduced by our group to study the charge extraction in the interfaces (Fig. 3c).[51] In this measurement, we use a nanosecond laser pulse to excite carriers in the perovskite layer. The excited carriers can be transferred in an adjacent charge-selective layer if present, causing a charge separation that is detectable as a surface photovoltage (SPV).This process induces a charge separation in the materials stack, that is detectable as the change in capacitance by a probe. An ideal trSPV signal exhibits a fast rise, indicating efficient charge injection of photogenerated carriers into HTL, followed by a slow decay, which suggests slow interfacial recombination and low defect density.[52,53] We measured transient SPV for both control (ITO/PEDOT/$Al_2O_3$/$FASnI_3$) and target (ITO/PEDOT/$Al_2O_3$/PEAI/$FASnI_3$) films. The initial rise and peak amplitude are similar for the two samples, with the signal amplitude of the target samples being slightly higher than the control sample. Importantly, the target samples show a significantly slower decay under all excitation wavelengths (Fig. 3d and e), indicating reduced trap density at the interface. Notably, the shape of the decay curves is similar for both samples (Fig. 3f), suggesting similar charge injection mechanisms. Overall, trSPV measurements confirmed the reduction in interfacial defects upon PEAI diffusion, as previously indicated by XRD, PL, and TRPL analyses, without altering the energy alignment.

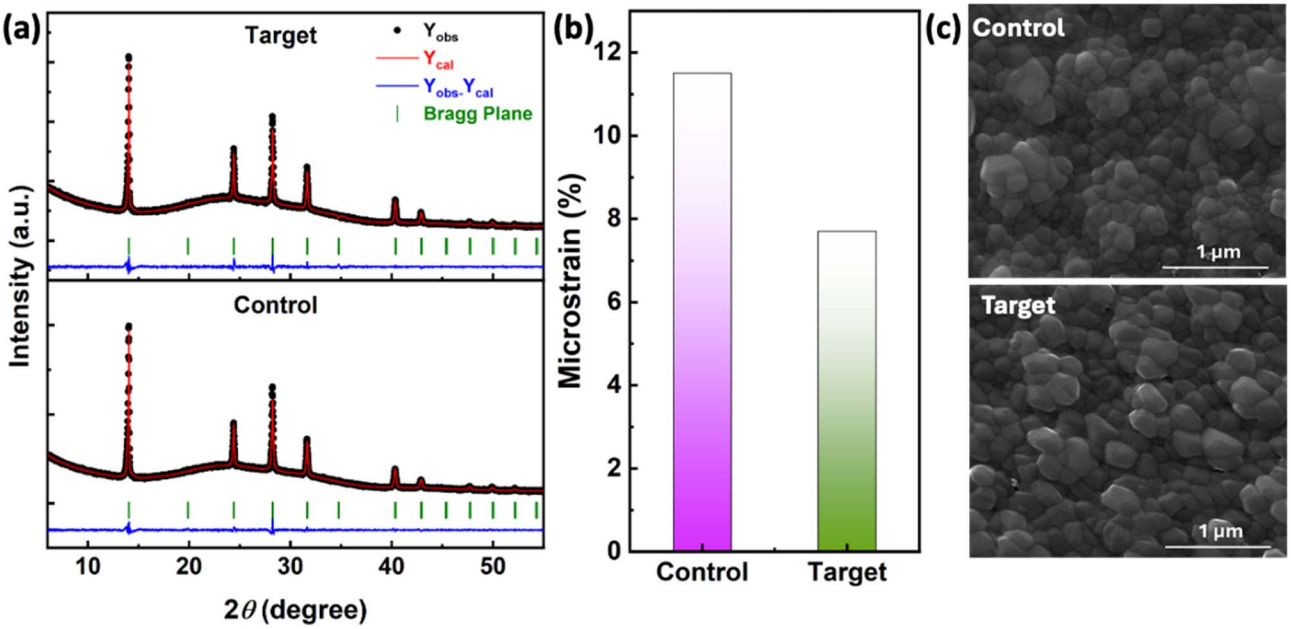


Fig. 2 Crystallographic and microstructural and analysis: (a) Le Bail fitting of X-ray diffraction patterns of control and target films. (b) Decrease in microstrain in target film upon introduction of PEAI interlayer. (c) Top view of SEM images of control and target films.

In order to investigate the recombination dynamics, space charge limited current (SCLC) method was explored by using p–n–p stack devices with the structure ITO/PEDOT/$Al_2O_3$/perovskite/PTAA/Ag and ITO/PEDOT/$Al_2O_3$/PEAI/perovskite/PTAA/Ag for both the control and target films respectively. There was an approximately 70% lower trap fill limit voltage ($V_{TFL}$) recorded for target device $V_{TFL} \approx 0.31$ V compared to control device where $V_{TFL} \approx 1.06$ V (Fig. S4a and b). The trape-

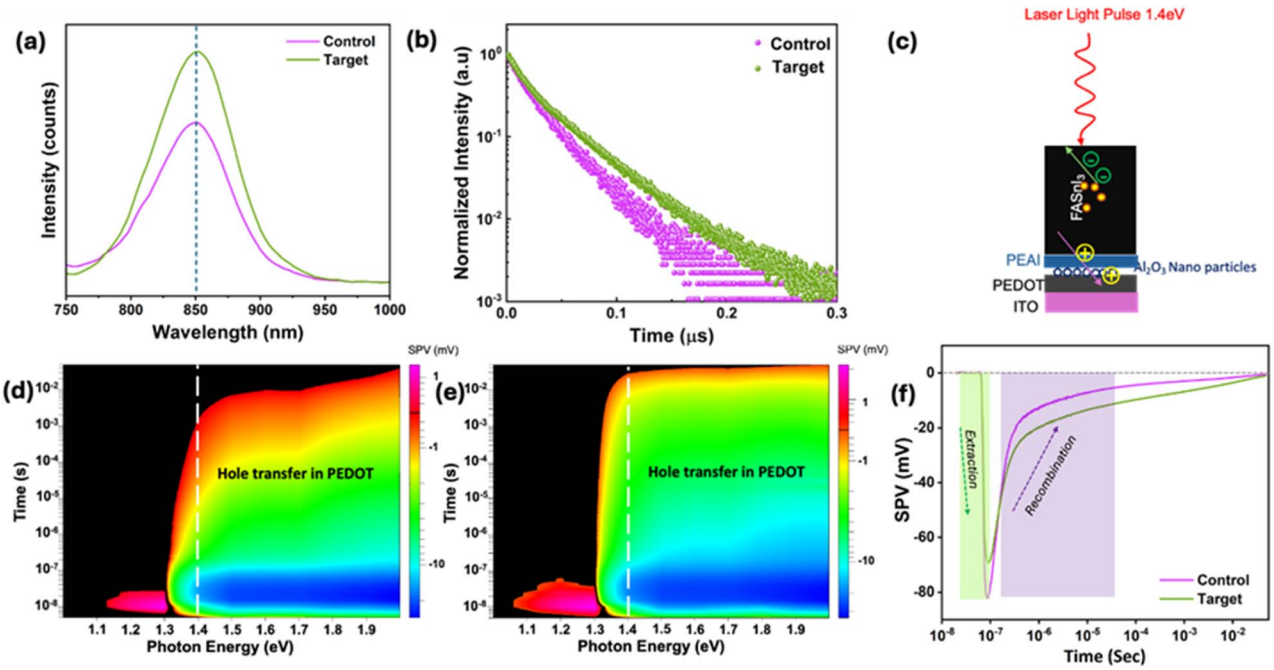


Fig. 3 Optical spectroscopy: (a) steady state photoluminescence spectroscopy measured for glass/$FASnI_3$ and glass/PEAI/$FASnI_3$ thin films. (b) Time-resolved photoluminescence (trPL) decay spectra of $FASnI_3$ and PEAI/$FASnI_3$ films (fitted spectra are shown in Fig. S3). (c) Charge extraction model and working principle of trSPV technique describing carrier transport to the PEDOT hole transport layer. Spectral dependence of transient SPV mapping, (d) $FASnI_3$, (e) PEAI/$FASnI_3$ on glass, demonstrated in contour plots. (f) trSPV measurements, at an excitation source of 885 nm (1.4 eV) with the light intensity of 1 sun illumination for $FASnI_3$ and PEAI/$FASnI_3$ films covered with glass on the top. The films were deposited on ITO/PEDOT/$Al_2O_3$ substrates. SCLC measurements of hole-only devices based on the perovskite films (g) control and (h) target.

state defect density ($N_{trap}$) for devices was reduced from 7.48 × $10^{16}$ $cm^{-3}$ to 1.24 × $10^{16}$ $cm^{-3}$. Consequently, these results confirms that the diffusion of PEAI into perovskite effectively passivates the defects located within the perovskite films and leads to a significant improvement in film quality, which is aligned with the previously stated PL, TRPL, and trSPV results.[54]

Finally, the solar cell devices were fabricated using the p–i–n configuration with device structure ITO/PEDOT-complex/$Al_2O_3$/PEAI/$FASnI_3$/$C_{60}$/BCP/Ag (Fig. 4a). First, to optimise the PEAI concentration, devices were fabricated with different concentrations of PEAI solutions such as 0.07, 0.1, and 0.5 M. Fig. S5 demonstrate that devices incorporating 0.5 M PEAI exhibited better photovoltaic performance among all tested concentrations. Fig. 4b represents the *J*–*V* curves of the best-performing control (without PEAI) and target (0.5 M PEAI) devices measured under 1-sun (AM 1.5G) illumination conditions. The champion control device exhibited a $J_{sc}$ of 21.4 mA $cm^{-2}$, a $V_{oc}$ of 0.6 V, FF of 70%, and an overall PCE of 8.9%. After the interface diffusion, the target devices achieved a state-of-the-art PCE of 11% for the DMSO-free tin perovskites with an enhanced $V_{oc}$ of 0.69 V, $J_{sc}$ of 21.3 mA $cm^{-2}$, and FF of 75% (Table S2). The observed $J_{sc}$ was also verified by the incident photon to current efficiency (IPCE) measurement where the integrated current density $J_{int}$ (Fig. 4c) and in agreement with the *J*–*V* measurement. The distribution of the photovoltaic parameters shows better statistics for target devices compared to control (Fig. 4d–g). Upon light exposure, the perovskite material generates electrons and holes, which are then transported to the electron transport layer (ETL) and HTL, respectively. However, some holes may become trapped at the interface due to the presence of undercoordinated ions and structural discontinuities that act as defects, leading to unwanted charge carrier accumulation. These trapped holes are more likely to recombine with free electrons, resulting in a loss of carriers and a decrease in photocurrent.[55–57] The incorporation of PEAI molecules at the interface effectively passivates these hole traps, reducing charge recombination and facilitating charge extraction at the interface. Interestingly, this approach led to enhancements in both Voc and FF, further indicating a reduction in interfacial defect density, which in turn governs the observed improvement in PCE. It is worth noting that the PCE of 11%

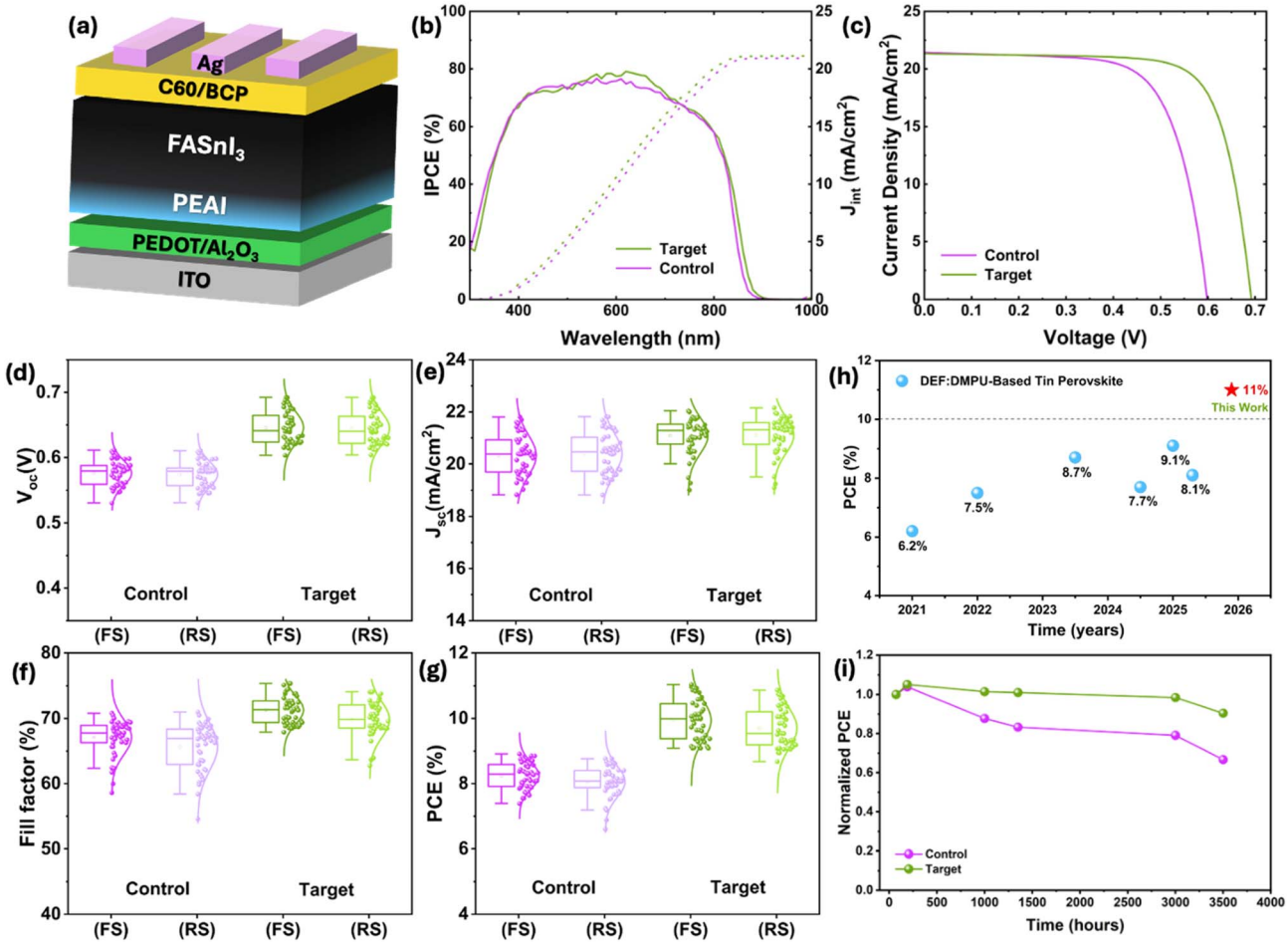


Fig. 4 Device performance under AM 1.5G illumination (1-sun): (a) Schematic of tin-PSC device architecture with pin configuration. (b) *J*–*V* curves of champion devices (control and target) in forward and reverse scan modes, and the corresponding (c) IPCE plots and integrated current density $J_{int}$. The box chart of 46 individual pixels in forward and reverse scans (d) $V_{OC}$, (e) $J_{SC}$, (f) FF, and (g) PCE for the control and target devices. (h) DEF : DMPU-based $FASnI_3$ devices reported previously (Table S3) and this work (red star mark). (i) Long-term stability in $N_2$ storage.

represents the highest value reported to date for DEF : DMPU-based tin PSCs (Fig. 4h).

Other than DEF : DMPU, there are some other solvent systems which have been reported for tin-PSCs processing. Our group used the mixture of dimethylformamide (DMF), 1,3-dimethyl-2-imidazolidinone (DMI), and 4-(*tert*-butyl) pyridine (tBP) and achieved maximum PCE of 7.8%.[58] Hayase and coworkers reported a PCE of 4.77% for DMSO-free tin perovskite using a mixture of DMF and 2-methyl-aminopyridine solvents.[59] Wakamiya and co workers have achieved a PCE of 11.6% using an antisolvent-free and DMSO-free approach where they used vacuum-quenching with crystal growth regulator (V-CGR) method for drying the perovskite film and a mixture of DMF and 1-vinylimidazole for tin perovskite processing.[60] In our work, we have achieved PCE of 11%, representing one of the leading performance for DMSO-free tin perovskite. In addition, the target devices exhibited a narrower hysteresis distribution, with an average hysteresis index (HI) of −0.01, compared to −0.14 for the control devices, as shown in (Fig. S6). The reduced hysteresis supports the role of PEAI in suppressing interfacial ion migration and stabilising interfacial energetics. Further, the target device exhibited low dark current compared to the control device, indicating reduced leakage current (Fig. S7).

Finally, we have explored the long-term stability of the DMSO-free devices for the first time under storage in a $N_2$ filled glovebox ($O_2$ < 0.1 ppm, $H_2O$ < 0.1 ppm) and continuous 1-sun illumination following the ISOS-1 protocol for stability measurement.[61] The PEAI-incorporated devices demonstrated outstanding stability, retaining approximately 90% of their initial PCE after 3500 hours of storage, whereas the control devices retained only around 80% (Fig. 4i). This superior stability was also reflected under continuous illumination, where the performance of both control and target devices was tracked for 500 hours (Fig. S8) under maximum power point. It is important to note that no reducing or scavenging agents were used in the perovskite precursor solution. Since a DMSO-free solvent system was employed, which does not oxidise $Sn^{2+}$, the intrinsic chemical stability of the perovskite layer was preserved, resulting in comparable operational stability between the control and target devices.

## Conclusion

We have improved the photovoltaic performance of DEF : DMPU-based tin perovskite solar cells by introducing a novel interface diffusion strategy. With this approach, we have achieved a record PCE of 11% for a non-oxidising solvent-based tin-PSCs. The enhanced device performance originates from improved crystallisation dynamics, as evidenced by the larger grain size and reduced lattice microstrain. This improved crystallinity results in a lower defect density, which is reflected by the higher stPL intensity and longer decay lifetime. The charger carrier dynamics are further verified by trSPV measurement, which shows slightly better charge extraction with much slower recombination upon PEAI buried interface modification. For the first time, we also investigated the long-term stability of DMSO-free tin PSCs devices, which retain approximately 90% of their initial power conversion efficiency after 3500 hours of storage without using any reducing or scavenging agents, revealing excellent stability. This highlights the intrinsic advantage of the non-oxidising solvent system in mitigating tin oxidation. We believe that these findings will stimulate further research on non-oxidising tin-based perovskites and interface modification, advancing the development of stable, efficient, and environmentally sustainable lead-free photovoltaic technologies.

## Conflicts of interest

There are no conflicts to declare.

## Data availability

We report the data in the supplementary information (SI). The reviewers can ask for more details. Supplementary information: detailed experimental methods, SEM images, trPL spectra, hysteresis index, dark *J–V*, and stability under maximum power point tracking. See DOI: https://doi.org/10.1039/d6el00022c.

## Acknowledgements

The authors thank the Distinguished Scientist Fellowship Program (DSFP) at KSU for financial support. The authors gratefully acknowledge the project LEAD-OUT-"POLYMER-SSISTED LEAD-FREE PEROVSKITE ASSEMBLY: TOWARDS ENVIRONMENTALLY-STAINABLE, HIGH-PERFORMANCE AND STABLE SOLAR CELLS" (Bando PRIN 2022-Italian Ministry of University and Scientific Research (MUR) Decreto Direttoriale 30 2023 prot. n. 966, project number 2022B3C94E) for funding. The authors gratefully acknowledge the project "Metal hAlide perovSkiTE single crystals for solaR cells" (MASTER) (Bando 2022 PNRR-Italian Ministry of University and Scientific Research (MUR) Decreto Direttoriale n. 1409 del 14-9-2022 Prot. P2022ZYTJY) for funding. This work was supported by the Italian Ministry of Environment and Energy Security in the framework of the Project GoPV (CSEAA_00011) for Research on the Electric System. We also acknowledge the Tin Cluster at HYSPRINT Photovoltaics lab, EMIL labs, and PVComB at HZB for characterisation and measurements.

## References

1 C. Li, A. Vincze, H. Park, F. Streller, K. Götz, S. Qiu, J. Byun, Y. Shang, Z. Yuan, L. Dong, J. Tian, Z. Peng, C. Liu, F. Yang, Y. Wang, A. Späth, A. Osvet, K. Forberich, T. Heumueller, S. H. Christiansen, M. Halik, R. H. Fink, T. Unruh, N. Li, L. Lüer and C. J. Brabec, *Energy Environ. Sci.*, 2025, **18**, 7660–7668.

2 Y. He, Y. Li, A. Gao, Q. Ren, Z. Liu, L. Chen, D. Wang and S. Liu, *Adv. Funct. Mater.*, 2025, **35**, 2502262.

3 J. Tong, Q. Jiang, F. Zhang, S. B. Kang, D. H. Kim and K. Zhu, *ACS Energy Lett.*, 2021, **6**, 232–248.

4 A. Kojima, K. Teshima, Y. Shirai and T. Miyasaka, *J. Am. Chem. Soc.*, 2009, **131**, 6050–6051.
5 B. Kazaishvili, *NREL Best Research-Cell PV Efficiency Chart*, 1976.
6 Y. Chen, H. T. Yi, X. Wu, R. Haroldson, Y. N. Gartstein, Y. I. Rodionov, K. S. Tikhonov, A. Zakhidov, X. Y. Zhu and V. Podzorov, *Nat. Commun.*, 2016, **7**, 12253.
7 Y. Wang, Y. Zhang, P. Zhang and W. Zhang, *Phys. Chem. Chem. Phys.*, 2015, **17**, 11516–11520.
8 M. H. Miah, M. U. Khandaker, M. B. Rahman, M. Nur-E-Alam and M. A. Islam, *RSC Adv.*, 2024, **14**, 15876–15906.
9 Y. Wang, Z. Feng, Y. Zhang, H. Huang, Y. Guo, J. Xu, H. Zhang, Y. Ji, L. Li, C. Ge, C. Huang, Y. Zhang, J. Sun, Y. Liu, X. Wu, X. Li, Y. Peng, S. Kang, S. Chen, W. Zhou, D. Tang, Y. Li, B. Ding, L. Zu, J. Z. Liu, K. Weber, X. He, N. Hu, Y. Cui, H. Zhan, X. Zhang and J. Peng, *Adv. Funct. Mater.*, 2026, **36**, e10458.
10 J. Li, H. L. Cao, W. Bin Jiao, Q. Wang, M. Wei, I. Cantone, J. Lü and A. Abate, *Nat. Commun.*, 2020, **11**, 310.
11 J. Tempowski, *WHO Guideline for Clinical Management of Exposure to Lead*, World Health Organization, 2021.
12 M. Lyu, J. H. Yun, P. Chen, M. Hao, and L. Wang, *Addressing Toxicity of Lead: Progress and Applications of Low-Toxic Metal Halide Perovskites and Their Derivatives*, Wiley-VCH Verlag, Vol. 7, 2017.
13 B. Chen, C. Fei, S. Chen, H. Gu, X. Xiao and J. Huang, *Nat. Commun.*, 2021, **12**, 5859.
14 C. H. Chen, S. N. Cheng, L. Cheng, Z. K. Wang and L. S. Liao, *Adv. Energy Mater.*, 2023, **13**, 2204144.
15 M. M. Byranvand, W. Zuo, R. Imani, M. Pazoki and M. Saliba, Tin-based halide perovskite materials: properties and applications, *R. Soc. Chem.*, 2022, **13**, 6766–6781.
16 A. Abate, Stable Tin-Based Perovskite Solar Cells, Vol. 8, *Am. Chem. Soc.*, 2023, **8**, 1896–1899.
17 F. Giustino and H. J. Snaith, *ACS Energy Lett.*, 2016, **1**, 1233–1240.
18 T. Li, X. Luo, P. Wang, Z. Li, Y. Li, J. Huang, Z. Jin, Y. Yang, B. Li, W. Zhang, S. Lin, Y. Rui, H. Wang, Q. Zhang, Y. Zhan, B. Xu, J. Liang and Y. Qi, *Nature*, 2025, **648**, 84–90.
19 T. Li, F. He, T. Shen, D. Yan, Z. Jin, B. Li, P. Wang, Z. Zhang, Z. Li, Y. Pu, L. Deng, L. Qin, W. Li, Y. Zhan, Z. Liu, Q. Fang, Y. Yao, Y. Liu, Y. Zhao, Y. Wang and J. Liang, *Nat. Energy*, 2026, **11**, 219–229.
20 D. He, P. Chen, J. A. Steele, Z. Wang, H. Xu, M. Zhang, S. Ding, C. Zhang, T. Lin, F. Kremer, H. Xu, M. Hao and L. Wang, *Nat. Nanotechnol.*, 2025, **20**, 779–786.
21 J. Xi and M. A. Loi, The Fascinating Properties of Tin-Alloyed Halide Perovskites, *Am. Chem. Soc.*, 2021, **6**, 1803–1810.
22 C. Frasca, P. Alippi, R. Schwiddessen, K. Prashanthan, G. Nasti, S. Zuo, M. O. Ur Rehman, M. H. Aldamasy, N. T. P. Hartono, A. Musiienko and A. Abate, *ACS Energy Lett.*, 2025, **10**, 526–533.
23 J. Pascual, G. Nasti, M. H. Aldamasy, J. A. Smith, M. Flatken, N. Phung, D. Di Girolamo, S. H. Turren-Cruz, M. Li, A. Dallmann, R. Avolio and A. Abate, *Mater. Adv.*, 2020, **1**, 1066–1070.
24 M. I. Saidaminov, I. Spanopoulos, J. Abed, W. Ke, J. Wicks, M. G. Kanatzidis and E. H. Sargent, Conventional Solvent Oxidizes Sn(II) in Perovskite Inks, *Am. Chem. Soc.*, 2020, **5**, 1153–1155.
25 Z. Zhang, J. Liang, J. Wang, Y. Zheng, X. Wu, C. Tian, A. Sun, Y. Huang, Z. Zhou, Y. Yang, Y. Liu, C. Tang and C. C. Chen, *Adv. Energy Mater.*, 2023, **13**, 2300181.
26 D. Di Girolamo, J. Pascual, M. H. Aldamasy, Z. Iqbal, G. Li, E. Radicchi, M. Li, S. H. Turren-Cruz, G. Nasti, A. Dallmann, F. De Angelis and A. Abate, *ACS Energy Lett.*, 2021, **6**, 959–968.
27 S. Covella, V. Armenise, M. O. Ur Rehman, E. Aktas, F. Fracassi, F. Palumbo, S. Colella, A. Abate and A. Listorti, *ACS Appl. Mater. Interfaces*, 2024, **37**, 49392.
28 D. P. Panda, R. Issaoui, Z. Iqbal, G. K. Grandhi, M. O. Ur Rehman, F. Zu, P. Alippi, M. Rastgoo, S. Zuo, E. Luzzi, M. Simmonds, L. Miele, L. Sanguigno, M. Li, P. Aprea, E. Di Maio, N. Koch, P. Vivo and A. Abate, *ACS Energy Lett.*, 2025, 3789–3798.
29 M. Zhu, S. Singh, A. M. C. Chong, J. M. Kim, F. Koc, D. P. Panda, P. Zimmermann, A. Hinderhofer, W. Luo, G. Alsabeh, M. O. Ur Rehman, G. Choi, D. Chernyshov, F. Schreiber, J. Y. Seo, Y. Vaynzof, A. Abate and J. V. Milić, *Adv. Energy Sustain. Res.*, 2025, **6**, 2500028.
30 H. Liu, Z. Zhang, W. Zuo, R. Roy, M. Li, M. M. Byranvand and M. Saliba, *Adv. Energy Mater.*, 2023, **13**, 2202209.
31 H. Dong, C. Ran, W. Gao, N. Sun, X. Liu, Y. Xia, Y. Chen and W. Huang, *Adv. Energy Mater.*, 2023, **13**, 2202209.
32 S. Jiao, T. Wang and Z. Zhou, *ChemSusChem*, 2025, **18**, e202500333.
33 H. Xu, Z. Liang, J. Ye, Y. Zhang, Z. Wang, H. Zhang, C. Wan, G. Xu, J. Zeng, B. Xu, Z. Xiao, T. Kirchartz and X. Pan, *Energy Environ. Sci.*, 2023, **16**, 5792–5804.
34 H. Guo, Y. Wang, K. Zhang, M. Tao, L. Guo, X. Zhang, Z. Song, J. Wen, T. Hou, Y. Huang and Y. Song, *Energy Environ. Sci.*, 2025, **18**, 7114–7123.
35 K. Chen, P. Wu, W. Yang, R. Su, D. Luo, X. Yang, Y. Tu, R. Zhu and Q. Gong, *Nano Energy*, 2018, **49**, 411–418.
36 M. Liao, B. Bin Yu, Z. Jin, W. Chen, Y. Zhu, X. Zhang, W. Yao, T. Duan, I. Djerdj and Z. He, *ChemSusChem*, 2019, **12**, 5007–5014.
37 M. Li, M. Li, M. Li, W. W. Zuo, W. W. Zuo, Y. G. Yang, M. H. Aldamasy, M. H. Aldamasy, Q. Wang, S. H. T. Cruz, S. L. Feng, M. Saliba, Z. K. Wang, A. Abate and A. Abate, *ACS Energy Lett.*, 2020, **5**, 1923–1929.
38 W. G. Choi, C. G. Park, Y. Kim and T. Moon, *ACS Energy Lett.*, 2020, **5**, 3461–3467.
39 C. Ran, J. Xi, W. Gao, F. Yuan, T. Lei, B. Jiao, X. Hou and Z. Wu, *ACS Energy Lett.*, 2018, **3**, 713–721.
40 A. Sattar, N. Shahzad, M. A. Tariq, T. Yousaf, S. Garcia-Ballesteros, M. I. Shahzad, R. Liaquat, M. Ali and F. Bella, *Mater. Today Energy*, 2025, **53**, 101986.
41 H. Zhu, W. Yang, Y. Reo, G. Zheng, S. Bai, A. Liu and Y. Y. Noh, *Nat. Electron.*, 2023, **6**, 650–657.
42 T. Wu, D. Cui, X. Liu, X. Luo, H. Su, H. Segawa, Y. Zhang, Y. Wang and L. Han, *Sol. RRL*, 2021, **5**, 2100034.

 

43 S. Li, X. Yang, S. Cheng, Y. Yang, H. Li, Z. Zheng, M. Li, Q. Yu, S. Yuan, Q. Lin and Z. Wang, *Nat. Commun.*, 2025, **16**, 8072.
44 T. H. Han, J. W. Lee, C. Choi, S. Tan, C. Lee, Y. Zhao, Z. Dai, N. De Marco, S. J. Lee, S. H. Bae, Y. Yuan, H. M. Lee, Y. Huang and Y. Yang, *Nat. Commun.*, 2019, **10**, 520.
45 S. Wang, C. Wu, H. Yao, L. Xie, Y. Xiao, L. Ding and F. Hao, *Small*, 2024, **20**, 2308877.
46 D. Bai, H. Wang, S. Yang, L. Duan, Y. Li, X. Zhu, S. F. Liu and D. Yang, *Adv. Energy Mater.*, 2025, **15**, 2501206.
47 Y. Ma, Q. Song, X. Yang, H. Zai, G. Yuan, W. Zhou, Y. Chen, F. Pei, J. Kang, H. Wang, T. Song, X. Wang, H. Zhou, Y. Li, Y. Bai and Q. Chen, *Nano Energy*, 2023, **108**, 108250.
48 D. K. Lee, K. Fykouras, T. Kodalle, R. F. Moral, C. P. Schwartz, N. Tamura, K. V. Lawler, L. Leppert and C. M. Sutter-Fella, *ACS Energy Lett.*, 2025, 1039–1049.
49 S. E. Fenni, M. R. Caputo, A. J. Müller and D. Cavallo, *Macromolecules*, 2022, **55**, 1412–1423.
50 D. Di Girolamo, E. Blundo, G. Folpini, C. Ponti, G. Li, M. H. Aldamasy, Z. Iqbal, J. Pascual, G. Nasti, M. Li, R. Avolio, O. Russina, A. Latini, F. Alharthi, M. Felici, A. Petrozza, A. Polimeni and A. Abate, *Sol. RRL*, 2022, **6**, 2100825.
51 Z. Iqbal, R. Félix, A. Musiienko, J. Thiesbrummel, H. Köbler, E. Gutierrez-Partida, T. W. Gries, E. Hüsam, A. Saleh, R. G. Wilks, J. Zhang, M. Stolterfoht, D. Neher, S. Albrecht, M. Bär, A. Abate and Q. Wang, *J. Am. Chem. Soc.*, 2024, **146**, 4642–4651.
52 T. Dittrich, S. Fengler and N. Nickel, *Phys. Status Solidi A*, 2021, **218**, 2100167.
53 Z. Iqbal, T. W. Gries, A. Musiienko and A. Abate, *Sol. RRL*, 2024, **8**, 2400329.
54 L. Zhang, G. Luo, W. Zhang, Y. Yao, P. Ren, X. Geng, Y. Zhang, X. Wu, L. Xu, P. Lin, X. Yu, P. Wang and C. Cui, *Adv. Sci.*, 2024, **11**, 2305582.
55 J. Kim and W. Jo, *Nano Converg.*, 2024, **11**, 57.
56 X. Sun, H. Wu, Z. Li, R. Zhu, G. Li, Z. Su, J. Zhang, X. Gao, J. Pascual, A. Abate and M. Li, *Angew. Chem., Int. Ed.*, 2024, **63**, e202409330.
57 N. Yan, Z. Fang, Z. Dai, J. Feng and S. Liu, *Adv. Funct. Mater.*, 2024, **34**, 2314039.
58 S. Zuo, A. Tarasov, L. Frohloff, K. Prashanthan, F. Ruske, M. Lounasvuori, C. Frasca, A. Dallmann, F. Zu, F. Mathies, F. Scheler, N. T. P. Hartono, G. Li, J. Li, M. Simmonds, W. Li, N. Koch, S. Albrecht, M. Li, E. Unger, M. H. Aldanmasy, A. Musiienko and A. Abate, *Adv. Sci.*, 2025, **12**, e01311.
59 T. Kitamura, S. Sasahara, S. Kani, J. Liu, H. Bì, S. R. Sahamir, G. Kapil, Y. Fujiwara, L. Wang, A. K. Baranwal, Q. Shen and S. Hayase, *ACS Appl. Energy Mater.*, 2025, **8**, 10891–10898.
60 F. Harata, R. Kaneko, S. Hu, N. Ohashi, T. Nakamura, M. A. Truong, R. Murdey and A. Wakamiya, *ACS Energy Lett.*, 2025, **10**, 5047–5056.
61 M. V. Khenkin, E. A. Katz, A. Abate, G. Bardizza, J. J. Berry, C. Brabec, F. Brunetti, V. Bulović, Q. Burlingame, A. Di Carlo, R. Cheacharoen, Y. B. Cheng, A. Colsmann, S. Cros, K. Domanski, M. Dusza, C. J. Fell, S. R. Forrest, Y. Galagan, D. Di Girolamo, M. Grätzel, A. Hagfeldt, E. von Hauff, H. Hoppe, J. Kettle, H. Köbler, M. S. Leite, S. F. Liu, Y. L. Loo, J. M. Luther, C. Q. Ma, M. Madsen, M. Manceau, M. Matheron, M. McGehee, R. Meitzner, M. K. Nazeeruddin, A. F. Nogueira, Ç. Odabaşı, A. Osherov, N. G. Park, M. O. Reese, F. De Rossi, M. Saliba, U. S. Schubert, H. J. Snaith, S. D. Stranks, W. Tress, P. A. Troshin, V. Turkovic, S. Veenstra, I. Visoly-Fisher, A. Walsh, T. Watson, H. Xie, R. Yıldırım, S. M. Zakeeruddin, K. Zhu and M. Lira-Cantu, *Nat. Energy*, 2020, **5**, 35–49.